iScience

CellPress
OPEN ACCESS

Article

Structures of activin ligand traps using natural sets of type I and type II TGFβ receptors

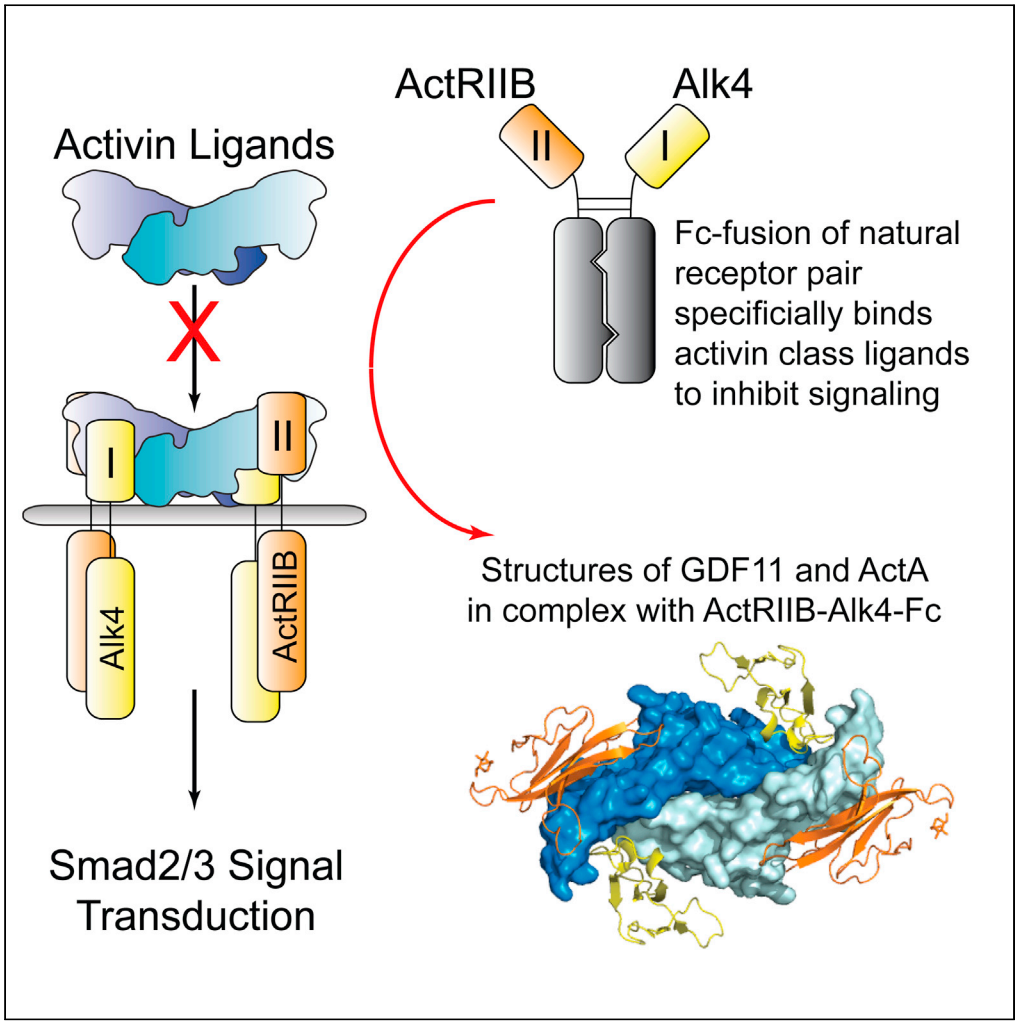

Erich J. Goebel, Chandramohan Kattamuri, Gregory R. Gipson, ..., Roselyne Castonguay, Ravindra Kumar, Thomas B. Thompson

Tom.Thompson@uc.edu

Highlights

Structure of type I and type II Fc receptor trap bound to TGF- β ligand

Similar ligand-binding interactions observed for low-affinity type I receptors

Structure of Alk4 reveals differences relative to other type I TGF-β receptors

Structures are consistent with the conformational selection model

Goebel et al., iScience 25, 103590
January 21, 2022
https://doi.org/10.1016/j.isci.2021.103590

iScience

CellPress
OPEN ACCESS

Article

Structures of activin ligand traps using natural sets of type I and type II TGFβ receptors

Erich J. Goebel,[1] Chandramohan Kattamuri,[1] Gregory R. Gipson,[1] Lavanya Krishnan,[2] Moises Chavez,[2] Magdalena Czepnik,[1] Michelle C. Maguire,[2] Rosa Grenha,[2] Maria Håkansson,[3] Derek T. Logan,[3] Asya V. Grinberg,[4] Dianne Sako,[2] Roselyne Castonguay,[2] Ravindra Kumar,[2] and Thomas B. Thompson[1,5,*]

SUMMARY

The 30+ unique ligands of the TGFβ family signal by forming complexes using different combinations of type I and type II receptors. Therapeutically, the extracellular domain of a single receptor fused to an Fc molecule can effectively neutralize subsets of ligands. Increased ligand specificity can be accomplished by using the extracellular domains of both the type I and type II receptor to mimic the naturally occurring signaling complex. Here, we report the structure of one "type II-type I-Fc" fusion, ActRIIB-Alk4-Fc, in complex with two TGFβ family ligands, ActA, and GDF11, providing a snapshot of this therapeutic platform. The study reveals that extensive contacts are formed by both receptors, replicating the ternary signaling complex, despite the inherent low affinity of Alk4. Our study shows that low-affinity type I interactions support altered ligand specificity and can be visualized at the molecular level using this platform.

INTRODUCTION

The transforming growth factor β (TGFβ) family includes more than 30 structurally similar ligands that play essential roles in animals, regulating embryonic development, adult tissue homeostasis, immune system function, and metabolic pathways (Hinck, 2012; Hinck et al., 2016; Weiss and Attisano, 2013). The family can be divided into three main classes based on sequence homology and canonical Smad activation: the TGFβs, activins, and bone morphogenetic proteins (BMPs). In each case, signaling occurs when a hexameric signaling complex is assembled consisting of a dimeric ligand together with two type I and two type II serine/threonine kinase receptors (Attisano et al., 1993; Wrana et al., 1994). A striking feature of the family is that 30+ ligands share just seven type I and five type II receptors. Thus, an extensive network of promiscuous interactions exists between ligands and receptors, with each receptor typically binding multiple distinct ligands and for many ligands, multiple receptors (Goebel et al., 2019a). For example, activin class ligand, growth differentiation factor 11 (GDF11), can utilize activin-like kinase 4 (Alk4), Alk5, or Alk7 as type I receptors, while the closely related ligand activin A (ActA) is limited to Alk4.

Structural and biochemical studies have defined the major signaling paradigms for each of the three classes, distinguished by differential receptor binding interfaces and affinities (Allendorph et al., 2006; Goebel et al., 2019b; Groppe et al., 2008). These observations, together with evidence that the activins display remarkable structural flexibility in their type I receptor-binding interface, have led to a proposed model of conformational selection in which minor changes in the type I receptor-binding site play major roles in receptor selectivity (Goebel et al., 2019a, 2019b). While these previous studies began to clarify the mechanisms underlying the assembly of activin class ligands and their receptors, we lack a full understanding of how the activin class ligands achieve specificity for type I receptors, in large part due to a lack of molecular information of how Alk4 interacts with the ligands. In fact, no structures of Alk4 have yet to be described, which could detail how Alk4 engages multiple, distinct activin class ligands and enables mechanistic comparisons across the activin class as a whole.

TGFβ family ligands are attractive targets for therapeutic strategies due to their roles in many biological processes and diseases. For example, multiple members of the activin class negatively regulate skeletal muscle mass, prompting efforts to inhibit their combined signaling for therapeutic benefits in the context of muscle wasting conditions (Latres et al., 2017; Li et al., 2021; Puolakkainen et al., 2017). One strategy for

[1]Department of Molecular Genetics, Biochemistry, and Microbiology, University of Cincinnati, 231 Albert Sabin Way ML 0524, Cincinnati, OH 45267, USA

[2]Acceleron Pharma, Inc., Cambridge, MA 02139, USA

[3]SARomics Biostructures AB, Medicon Village, Scheeletorget 1, 223 63, Lund, Sweden

[4]Dragonfly Therapeutics, Waltham, MA 02451, USA

[5]Lead contact

*Correspondence: Tom.Thompson@uc.edu

https://doi.org/10.1016/j.isci.2021.103590

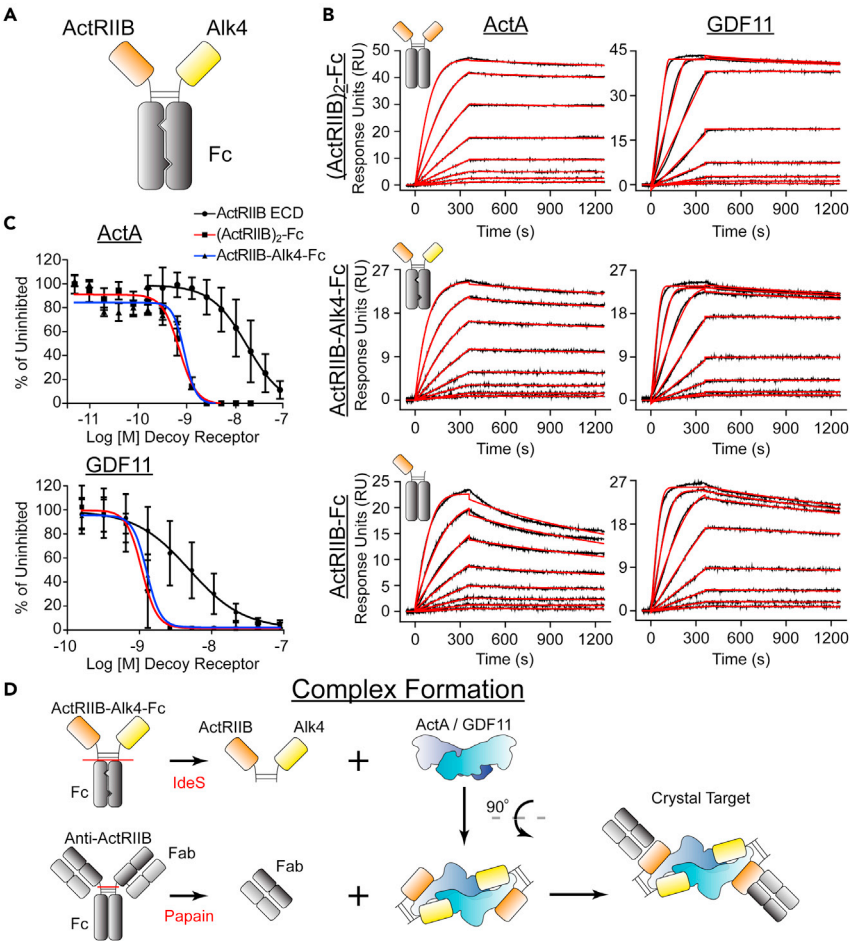

Figure 1. Characterization of ActRIIB-Alk4-Fc

(A) Domain structure of the decoy receptor platform, ActRIIB-Alk4-Fc.

(B) SPR sensorgrams of ActA and GDF11 binding to anti-human antibody-captured $(ActRIIB)_2$-Fc, ActRIIB-Alk4-Fc, or ActRIIB-Fc. Sensorgrams (*black lines*) are overlaid with fits to a 1:1 interaction model with mass transport limitations (*red lines*). Each experiment was performed in triplicate and the kinetic parameters are summarized in Table S1.

(C) Luciferase reporter assay showing the inhibitory activity following titration of ActRIIB-ECD, homodimeric $(ActRIIB)_2$-Fc, or ActRIIB-Alk4-Fc against a constant concentration (0.62nM) of ActA or GDF11 in HEK293 $(CAGA)_{12}$ cells. Each data point represents the mean ± SD of duplicate experiments measuring relative luminescence units (RLU).

(D) Schematic representation of the stepwise process of generating the ligand/receptor complex.

concerted multiligand inhibition employs soluble receptor-based traps, which inhibit signaling by ligand sequestration. A homodimeric Fc-fusion construct containing two copies of the activin receptor type IIB (ActRIIB) extracellular domain (ECD) fused with the human IgG1 Fc domain ($(ActRIIB)_2$-Fc) was found to neutralize multiple activin class ligands and increase muscle mass robustly in preclinical animal studies (Puolakkainen et al., 2017; Sako et al., 2010). To address the potential vascular complications arising from inhibition of the BMP class member, BMP9, a heterodimeric Fc-fusion construct was generated containing ECDs from ActRIIB and Alk4 (ActRIIB-Alk4-Fc), a naturally occurring signaling pair tethered together in a single molecule (Figure 1A) (Li et al., 2021). This heterodimeric agent selectively inhibits the signaling of activin class ligands ActA, ActB, GDF8, and GDF11 without BMP9 inhibition and improves muscle mass, function, and related attributes in murine disease models. A more complete understanding of how ActRIIB-Alk4-Fc interacts with target ligands at the molecular level could facilitate the future development of variants with improved therapeutic potential.

Historically, it has been difficult to ascertain structural information regarding the activin type I receptors—and, by extension, full activin receptor complexes—in large part due to the low-affinity interaction between

activin class ligands and their type I receptors, which impedes the formation of a stable ligand–receptor complex necessary for generating crystal structures. Thus, we hypothesized that using the ActRIIB-Alk4-Fc molecule, which tethers the low affinity type I receptor and the high affinity type II receptor, would stabilize the lower affinity interactions and reveal structural information for how Alk4 binds to activin ligands. In this study, we present the structures of two different activin class ligands, ActA and GDF11, in complex with ActRIIB-Alk4-Fc, representing the first structures of Alk4 and of this heterodimeric therapeutic candidate. Our results detail key structural features by which Alk4 selectively accommodates and engages multiple activin class members, thus sorting them from the broader milieu of TGFβ family ligands and providing a structural basis for their combinatorial signaling in muscle homeostasis and disease.

RESULTS

ActRIIB-Alk4-Fc binds to and inhibits ActA and GDF11 with high affinity

ActRIIB-Alk4-Fc was generated through co-expression of two human IgG1 Fc fusion constructs: one of the extracellular (ECD) domain of human ActRIIB (19–134) and another of human Alk4 ECD (24–126) and a C-terminal 6x His tag. The CH3 domains of each Fc were optimized through mutagenesis to minimize homodimer formation (Figure 1A) (Li et al., 2021). Each receptor ECD was joined to the antibody hinge region with a 4 amino acid linker, TGGG. Conditioned media from CHO cells incubated with kifunensine was subjected to tandem affinity purification using Protein A, Ni Sepharose, and an ActRIIB-specific affinity column (Li et al., 2021). This process efficiently separated the Fc-homodimers (Alk4-Fc and ActRIIB-Fc) from the heterodimer ActRIIB-Alk4-Fc with the purified protein validated through mass spectrometry.

In order to determine if the Alk4-ECD is involved in ligand binding, we used surface plasmon resonance (SPR) to measure the binding affinities of ActRIIB-Alk4-Fc to the ligands, ActA and GDF11, along with a comparison to two decoy receptor constructs: a homodimeric $(ActRIIB)_2$-Fc and a Fc fusion construct consisting of a single ActRIIB extracellular domain (ActRIIB-Fc) (Figure 1B, Table S1). If the Alk4-ECD was contributing to binding, we would expect ActRIIB-Alk4-Fc to have a higher affinity than ActRIIB-Fc for each ligand but would be weaker than the Fc construct that incorporates both high affinity receptors, $(ActRIIB)_2$-Fc. As expected, for both ActA and GDF11, binding affinity was highest for $(ActRIIB)_2$-Fc (equilibrium constants (apparent K_D) of 12.5 and 1.91pM for ActA and GDF11, respectively) followed by that of ActRIIB-Alk4-Fc (30.4 and 4.24pM) and ActRIIB-Fc (108 and 14.7pM). This data support that when compared with ActRIIB-Fc, the addition of an Alk4 extracellular domain in ActRIIB-Alk4-Fc enhances ligand binding and is only slightly weaker than $(ActRIIB)_2$-Fc.

Next, we investigated the capacity of the decoy receptor constructs, particularly ActRIIB-Alk4-Fc, to inhibit ligand signaling. Here, we used a HEK293T cell-line that is stably transfected with a luciferase under a SMAD2/3 responsive promoter ($(CAGA)_{12}$), which we have used to assay both ActA and GDF11 previously (Goebel et al., 2019b; Kumar et al., 2021). Signaling from ActA or GDF11 was inhibited by the titration of various decoy receptors (Figures 1C and S1). ActRIIB-Alk4-Fc and $(ActRIIB)_2$-Fc were both potent inhibitors of ActA and GDF11, suggesting little to no loss in the inhibitory capacity with the replacement of one ActRIIB-ECD with that of Alk4-ECD. Further, both fusion constructs were significantly more inhibited than the single high-affinity receptor, ActRIIB-ECD, or the single-substituted ActRIIB-Fc. Taken together with the SPR data, these experiments indicate that the Alk4-ECD is contributing to the high-affinity ligand binding and neutralization by the heterodimeric decoy receptor.

Crystallographic structures of ActRIIB-Alk4 bound to ActA and to GDF11

Crystallographic studies of low-affinity type I receptors within the activin family have been challenging. Thus, we reasoned that the fusion of both the type I and type II receptors in a single construct might provide an opportunity to trap the low-affinity receptor in a crystal lattice. Initial efforts to crystallize the full-length ActRIIB-Alk4-Fc ligand complex were not successful. Therefore, a smaller complex was generated by removing the constant Fc fragment, below the hinge region with the IdeS protease, keeping the receptors tethered through two disulfide bonds (Figure 1D). Complexes were subsequently formed with either ActA or GDF11, but again failed to produce crystals. Diffraction quality crystals were only obtained after the addition of a non-neutralizing Fab fragment that binds to ActRIIB. The antibody was originally selected for by binding to ActRIIB in the presence of ligand and thus does not interfere with ligand binding. Additionally, N- and O- linked glycans were removed through enzymatic treatment following complex formation. The Fab fragment of the antibody was isolated through papain cleavage and subsequently combined

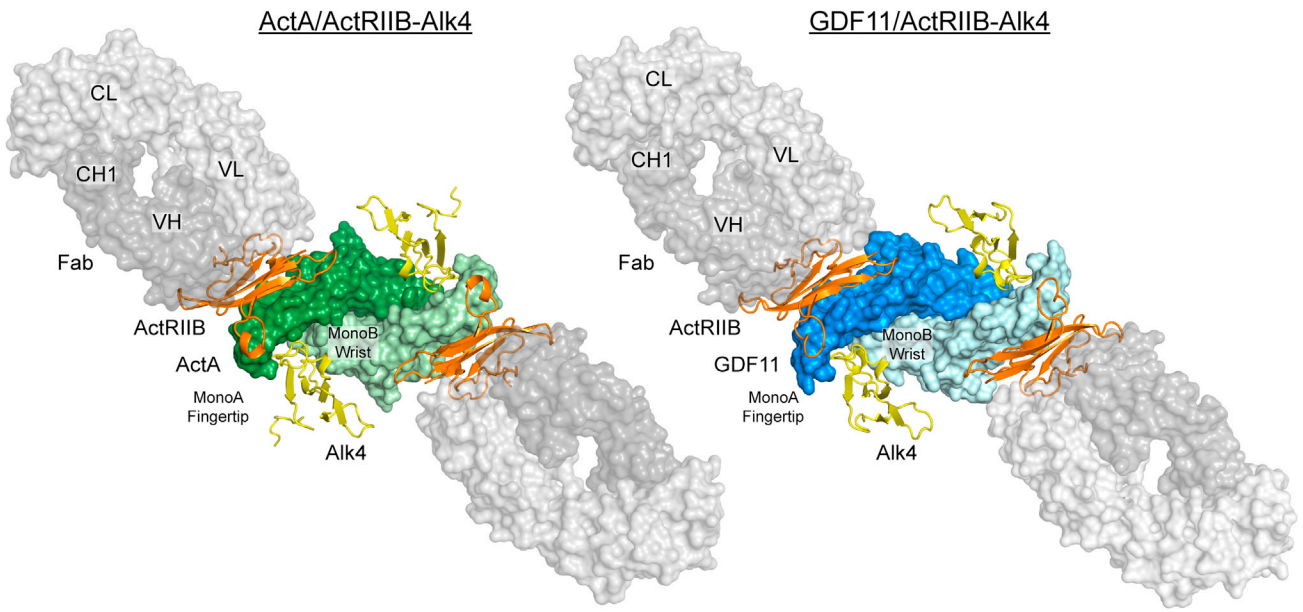

Figure 2. Structures of ActA/ActRIIB: Alk4/anti-ActRIIB Fab and GDF11/ActRIIB: Alk4/anti-ActRIIB Fab

Each ligand has two monomers represented in different shades of *green* (ActA, PDB: 7OLY) or *blue* (GDF11, PDB: 7MRZ) with ActRIIB-ECD represented in *orange*, Alk4-ECD in *yellow*, and the Fab molecules in two shades of *gray*. ActRIIB binds at the convex region of both ligands, whereas Alk4 binds at the concave, composite interface formed from surfaces on both monomers.

with the ligand/ActRIIB-Alk4 complexes, generating the final complex (Figure 1D), which yielded several crystallographic hits for both complexes: ActA/ActRIIB-Alk4 and GDF11/ActRIIB-Alk4. Detailed methodologies for the generation and purification of the complexes can be found in STAR Methods and in Figure S2.

Structures of the ActA/ActRIIB-Alk4/Fab and GDF11/ActRIIB-Alk4/Fab were solved to 3.26Å and 3.0Å resolution, respectively, through molecular replacement using search models built from previously resolved structures (ActA, GDF11, ActRIIB). Search models for Alk4 and the anti-ActRIIB Fab were built from modeling to most sequentially homologous type I receptor, Alk5 (6MAC), and Fab (6ATT for GDF11 and 5K59 for ActA complex) (data collection and refinement statistics are provided in Table S2) (Goebel et al., 2019b; Oganesyan et al., 2018). The asymmetric unit for both complexes contains one ligand monomer, one ECD of ActRIIB and Alk4, and one Fab fragment with the complete signaling complex present through crystallographic symmetry (Figure 2). Of note, the unit cell of each crystal lattice was greater than 975Å in the c-axis, where only a handful of protein crystal structures have similar or longer dimensions. This long dimension is shown in Figure S3 along with the corresponding crystal contacts that are mainly through the Fab fragment, which self-assembles to form a scaffold for the ligand/receptor complexes.

Similar placement of the receptors is observed in both structures where ActRIIB binds at the convex ligand interface and Alk4 binds within the concave interface built from surfaces on both ligand monomers. As expected, ActRIIB and Alk4 adopt a three-finger toxin fold and bind independently with no inter-receptor contacts. This overall receptor positioning is similar to that of the previously resolved activin and BMP receptor complexes (Allendorph et al., 2006; Goebel et al., 2019b; Townson et al., 2012; Weber et al., 2007). Electron density was well defined for the following residues in ActA/ActRIIB-Alk4: ActA (311–426), ActRIIB (26–120), Alk4 (31–109), Anti-ActRIIB Fab (1–220), and in GDF11/ActRIIB-Alk4: GDF11 (300–407), ActRIIB (25–120), Alk4 (31–105), Anti-ActRIIB Fab (1–222). Several C-terminal residues of both ActRIIB (121–134) and Alk4 (110–126), including the disulfide linker, did not have density and were not modeled. The distance between the C-terminal tails of each receptor was measured. With two receptors of each type binding to the dimeric ligand, cis receptors are defined as those interacting with the fingertips of the same chain while *trans* receptors are arranged across the length of the dimer. For GDF11 and ActA, the distance between tails for the receptor in the cis position is 42 Å and 55 Å while in the *trans* it is 57 Å and 66 Å, respectively. While not conclusive, this hints that the cis receptors are tethered in the structure. However, the missing

residues of the linker (44) are sufficient to support both conformations. Furthermore, the linker would have to extend around the N-terminus of the ligand to connect the receptors in the *trans* configuration, providing additional support to the likelihood of a cis configuration.

ActRIIB engages both ActA and GDF11 through the use of a centralized hydrophobic triad (Tyr^{60}, Trp^{78}, Phe^{101}), with little difference in orientation or conformation between the two receptor complexes (RMSD = 0.80 over Cα atoms). Despite this similarity, the GDF11/ActRIIB interface area is larger than that of ActA (770 $Å^2$ vs. 696 $Å^2$), consistent with the SPR data, which shows a stronger affinity between ActRIIB-Fc and GDF11 as well as previous crystal structures (Goebel et al., 2019b; Greenwald et al., 2004; Thompson et al., 2003). Each ActRIIB molecule is also bound by both the VH and VL domains of the anti-ActRIIB Fab, with the VH domain contributing the bulk of the interfacial area, ~80% in both structures. Comparison with previous structures of ActRIIB in complex with ActA or GDF11 revealed no major conformational changes occur upon binding of the Fab to the ActRIIB (e.g. RMSD = 0.75 Å over 95 Cα atoms, structural alignment to ActRIIB in PDB 6MAC, or 0.79 over 92 Cα atoms, alignment to ActRIIB in PDB 1NYU) (Goebel et al., 2019b; Thompson et al., 2003).

Alk4 binding to activin A and GDF11

The crystal structures of ActA/ActRIIB-Alk4 and GDF11/ActRIIB-Alk4 represent the first molecular characterization of Alk4 at the atomic level. Alk4 is positioned in the concave, composite interface, forming contacts with both ligand monomers (MonoA and MonoB) (Figure 3A). While the buried surface area between Alk4 and MonoA is similar between ActA and GDF11 (383.1 $Å^2$ and 365.5 $Å^2$, respectively), a significant difference in the interface between Alk4 and MonoB is observed where more surface area is buried in complex with ActA (586.6 $Å^2$ and 371.2 $Å^2$, for ActA and GDF11, respectively) (Figure S4).

Given these differences, we next wanted to compare the binding interfaces of Alk4 with both ActA and GDF11. Mapping of both the common and the unique Alk4 residues that participate in the interaction with the ligands reveals a common utilization of the β4β5 loop by both ActA and GDF11 (Figure 3B). This feature is generally conserved in all TGFβ family ligand/type I receptor interactions including receptor complexes with both BMP and TGFβ ligands (Allendorph et al., 2006; Groppe et al., 2008; Radaev et al., 2010; Townson et al., 2012; Weber et al., 2007). A comparison of the interactions between the Alk4 β4β5 loop and both ActA and GDF11 are shown in Figure 3C. At the center of this interface, Phe^{82} forms a knob-in-hole interaction with a hydrophobic pocket built from residues in both monomers, such as the two TGFβ family conserved tryptophan residues on MonoA and either Phe^{368} in ActA or Pro^{354} in GDF11 at the N-terminus of the wrist helix of MonoB (Figure 3C). Interestingly, Phe368 is conserved in ActA, ActB, ActC, and ActE, while Pro^{354} is conserved in both GDF8 and GDF11. Additionally, Lys80 from Alk4 contributes to a pi-stack with Trp^{337} in ActA or Trp329 in GDF11. Further contacts are observed at the ligand fingertip where an aspartate residue in both ActA and GDF11 residue forms a hydrogen bond with Gly79 of the Alk4 β4β5 loop. These interactions are a result of the fingertips curling toward the type I receptor, a feature that is not observed with BMP or TGFβ ligands (Allendorph et al., 2006; Groppe et al., 2008; Radaev et al., 2010; Townson et al., 2012; Weber et al., 2007).

While ActA and GDF11 bind the β4β5 loop similarly, significant differences are observed with how each ligand interacts with the β3β4 region of the receptor, which is engaged by the wrist helix of the ligand, including the prehelix loop (Figure 3B). A significant difference between ActA and GDF11 is the size and composition of the prehelix loop, which is eight amino acids longer in ActA. These differences result in differential interactions of each ligand with Alk4 accounting for the differences in surface area of the ligands with MonoB. Figure 3D shows the comparison of how the ActA and GDF11 prehelix loop packs into the Alk4 β3β4 region. With ActA, the prehelix engages two locations spanning opposite ends of the β3β4 strands including the β3β4 loop. These unique contacts are also shown in Figure 3B, plotted on Alk4. In contrast, the prehelix of GDF11 is positioned further away and only contacts residues across the center of the β3β4 strands, relying on van der Waals interactions. The additional contacts formed by the ActA prehelix, notably a saltbridge between His357 and Glu63 in Alk4, facilitates a conformational difference in the β3β4 loop. Additionally, the prehelix extension positions Ser362 and Ser365 for hydrogen bond formation with Alk4 residues, Glu74 and Tyr83, respectively. The latter is also flanked by favorable hydrophobic interactions with Phe368 of the ActA prehelix (Figure 3D). Thus, the greater surface area utilization of ActA is a result of increased interactions between the prehelix and the β3β4 region of Alk4.

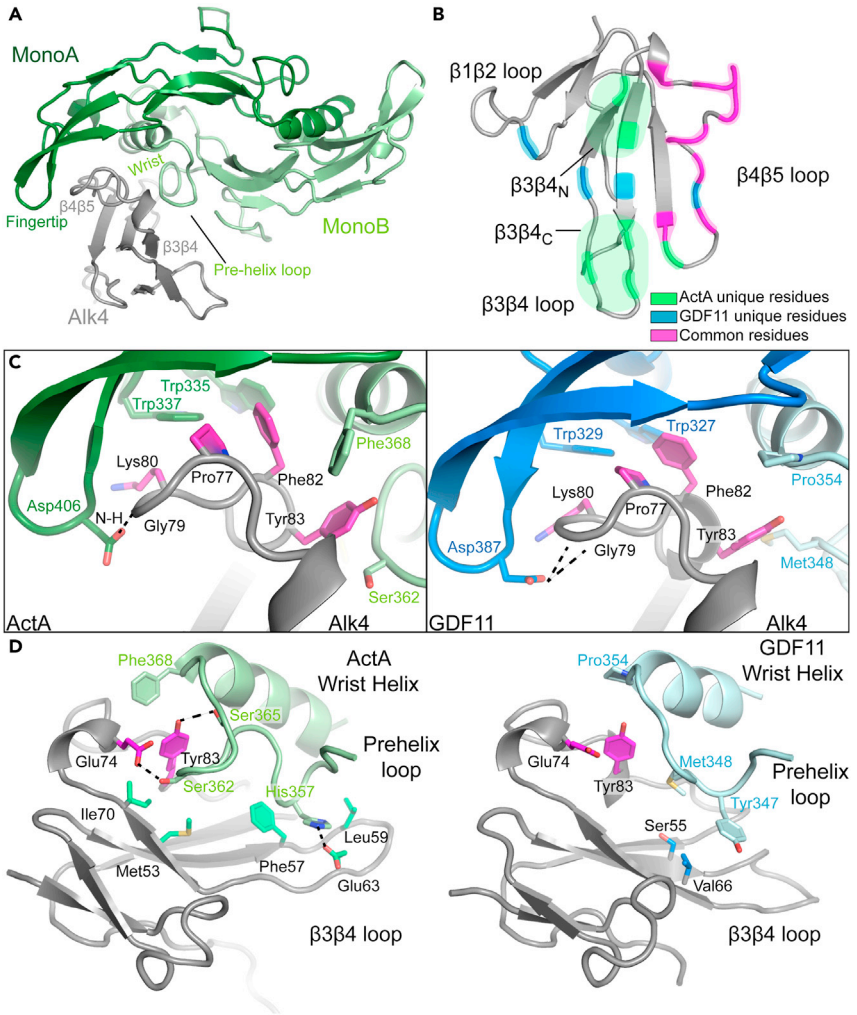

Figure 3. Binding of Alk4 to ActA and GDF11

(A) Cartoon representation of ActA (*green*) bound to Alk4 (*gray*).

(B) Alk4 colored to highlight amino acids utilized during binding to ActA (*green*), GDF11 (*blue*), or shared between the two ligands (*magenta*).

(C) Specific molecular interactions between the Alk4 β4β5 loop and the fingertip 2 of ActA (*left*) and GDF11 (*right*).

(D) Interactions between the Alk4 β3β4 loop and the prehelix region of ActA (*left*) and GDF11 (*right*). For *C* and *D*, colored residues match the scheme form (B)Of note, density is not obvious for Phe^{82} for the GDF11 structure, although the surrounding mainchain and residues are apparent. Owing to steric clashes, only one acceptable rotamer is possible, thus we have modeled Phe^{82} sidechain in a similar position as the activin structure.

Comparison of Alk4 to other TGFβ family type I receptors

While the general fold of the TGFβ type I receptors is similar, previous studies have indicated that differences in each structure play a role in ligand binding and specificity (Goebel et al., 2019a, 2019b; Kotzsch et al., 2009; Nickel et al., 2005; Salmon et al., 2020; Townson et al., 2012). In total, there are 7 type I receptors that are canonically classified into two clades: Alk1, Alk2, Alk3, and Alk6 which signal through Smad1/5/8 (BMP) and Alk4, Alk5, and Alk7 signaling through Smad2/3 (Activin and TGFβ). Of these receptors, several have been structurally resolved: Alk1, Alk3, Alk5, and Alk6, each of which has been characterized in a ligand/receptor complex (Goebel et al., 2019b; Groppe et al., 2008; Kotzsch et al., 2009; Townson et al., 2012; Weber et al., 2007; Zuniga et al., 2005). With the resolution of the Alk4 complex structures, we now have multiple resolved type I receptors that signal through Smad2/3, allowing for a structural comparison to receptors that signal through Smad1/5/8 (Figure 4).

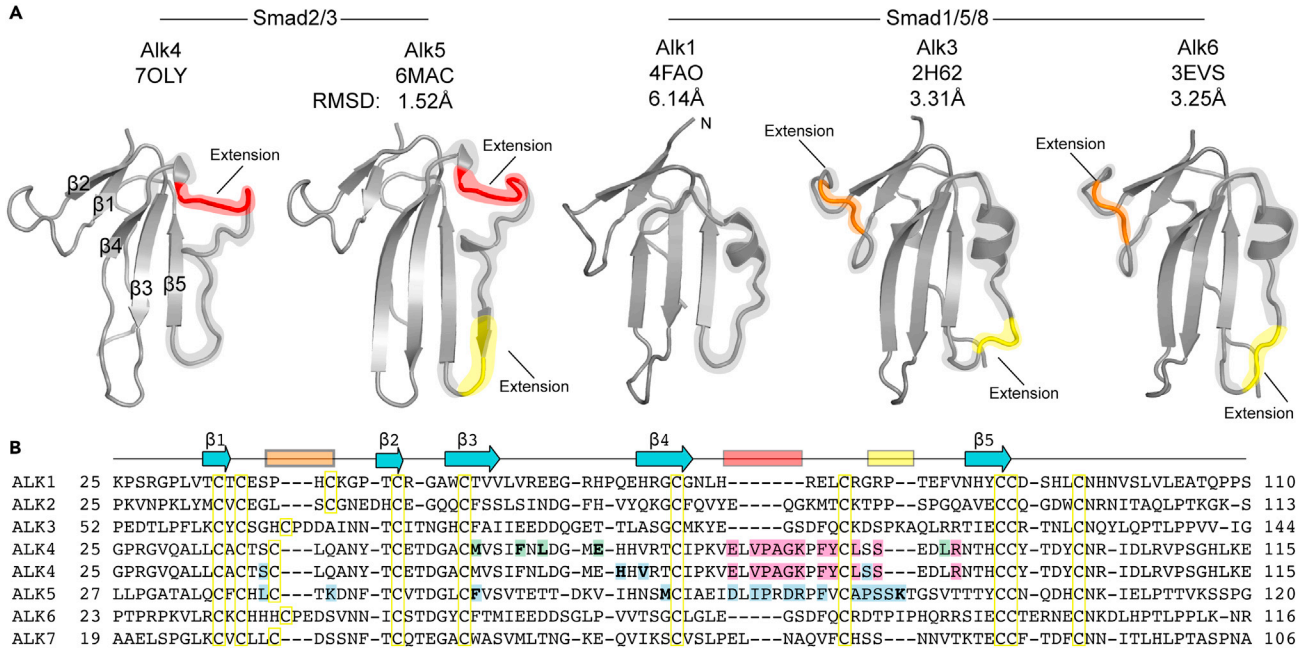

Figure 4. Ligand bound type I receptor cross comparison

(A and B) (A) Structures of Alk1 (PDB: 4FAO), Alk3 (2H62), Alk6 (3EVS), Alk4 (7OLY), and Alk5 (6MAC) (Goebel et al., 2019b; Kotzsch et al., 2009; Townson et al., 2012; Weber et al., 2007). RMSD calculations performed on Cα atoms through Pymol align and in relation to Alk4 (7OLY). Regions of relative extension are colored *orange*, *red*, or *yellow* and correspond to secondary structure regions highlighted on: (B) sequence alignment of the type I receptors. Cysteine residues are boxed in *yellow*, Alk4 residues unique to interaction with ActA are highlighted in *green*, while Alk4 and Alk5 residues unique to interaction with GDF11 are highlighted in *blue* for comparison. Alk4 residues that interact with both ActA and GDF11 are highlighted in *pink*. Residues that interact with the ligand prehelices are *bold*.

Alignment of each of the type I receptors reveals several loop extensions and conformational differences in the components that interact with the ligands. One difference occurs in the β1β2 loop, which is extended in the BMP receptors, Alk3 and Alk6, and contributes significantly to ligand interactions (Allendorph et al., 2006; Kotzsch et al., 2009; Weber et al., 2007). This extension is not present in Alk4 or Alk5 and no major interactions are observed between this region and the activin ligands (Figure 4B). However, the most striking difference occurs within the β4β5 loop, where members of the Smad1/5/8 clade possess anα-helix in the N-terminal portion of the loop. Interestingly, this secondary structure element is formed upon ligand binding in Alk3, as it is not present in the unbound states (Klages et al., 2008). Both Alk4 and Alk5 deviate from Alk1, Alk3, and Alk6 by sharing a five amino acid extension of the N-terminal portion of the β4β5 loop with limited secondary structure elements observed in either bound (Alk4 and Alk5) or unbound (Alk5) states. The protrusion of the β4β5 loop in Alk4 and Alk5, as a result of the extension, facilitates interaction with the ligand fingertip, as seen in each of the activin complex structures, whereas structures of BMP ligand/receptor complexes do not share this feature. Interestingly, while Alk4 and Alk5 are highly similar (RMSD: 1.52 Å over 76 Cα atoms, structural alignment to PDB 6MAC), Alk4 has a shorter β4β5 C-terminal region, which is extended by three residues in Alk5 (Figure 4B) (Goebel et al., 2019b). Alk5 shares this extension with Alk3 and Alk6, which has been shown to form important contacts with the ligand (Allendorph et al., 2006; Kotzsch et al., 2009; Weber et al., 2007). Both Alk4 and Alk5 share a cis proline (Pro^{77} for Alk4 and Pro^{55} for Alk5) at the N-term of the β4β5 loop, which was shown to be important for the conformation of this loop in the unbound state of Alk5 and important for ligand binding (Zuniga et al., 2011). Taken together, the cross comparison of type I receptors shows that structural differences, including insertions, play a role in forming unique contacts with specific ligands to impact signaling specificity.

Structural and functional comparison of Alk4 and Alk5

Previously, structural studies have illuminated a type I receptor specificity element in the BMP prehelix loop, where BMP2 can signal through Alk3 and Alk6, while a single arginine residue, present in GDF5

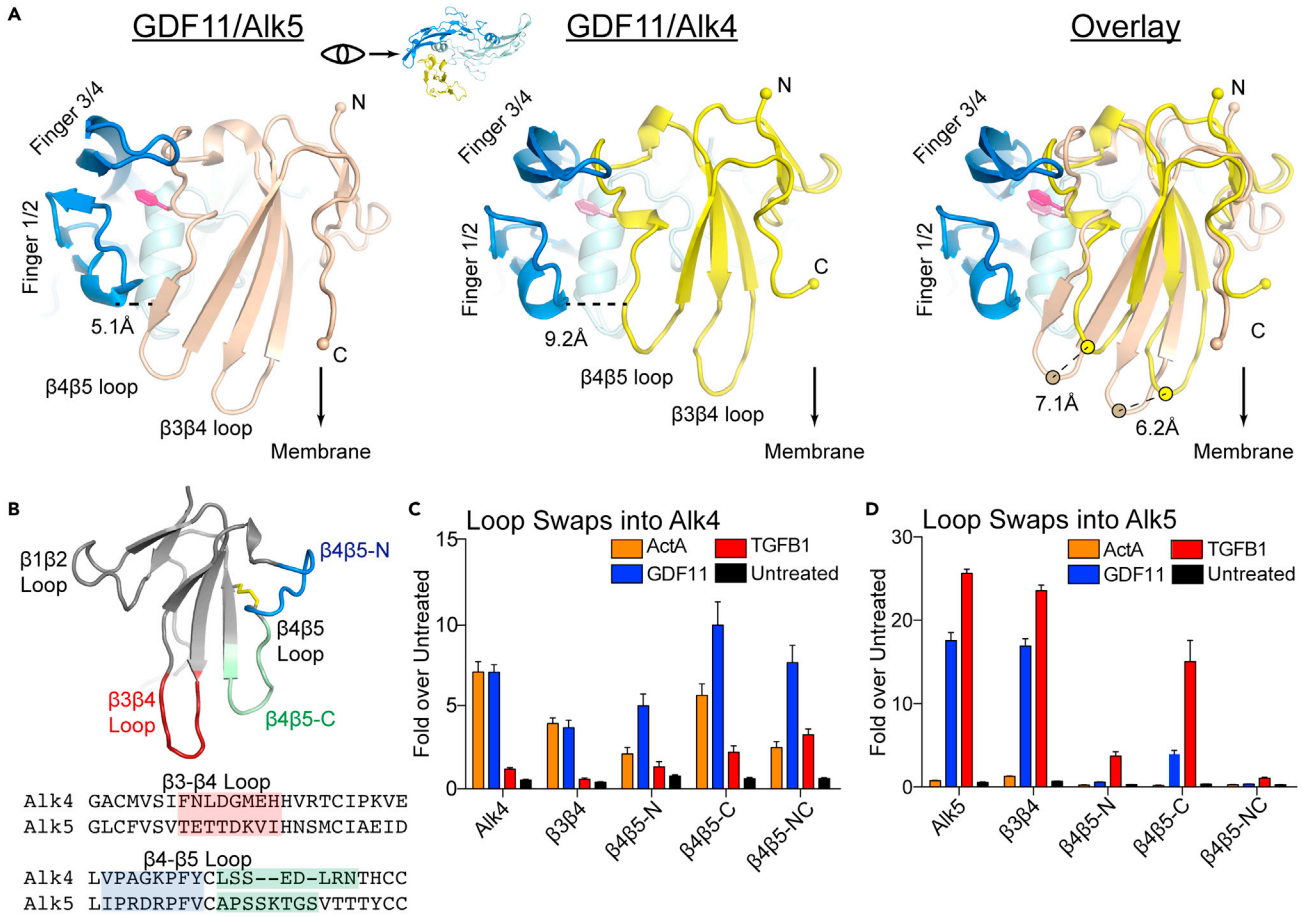

Figure 5. Differential Alk4 and Alk5 binding and region swaps

(A) Comparison of GDF11 (*blue*) binding to Alk5 (PDB: 6MAC, *wheat*) and Alk4 (*yellow*) in relation to the cell membrane (Goebel et al., 2019b). Anchoring phenylalanine shown in shades of *pink* for emphasis.

(B) Alk4 with the β3β4 loop (*red*), β4β5 N-term (*blue*), and C-term (*green*) regions of the β4β5 loop highlighted. Disulfide bond in the middle of the β4β5 is represented in *yellow*. *Bottom*: sequence alignment of the β3β4 and β4β5 loops with amino acids highlighted accordingly.

(C and D) Luciferase reporter assay showing the effects of mutational swaps of the Alk5 regions into Alk4 (C) and the corresponding Alk4 regions into Alk5 (D). Each data point represents the mean ± SD of triplicate experiments measuring relative luminescence units (RLU).

prevents binding to Alk3, suggesting that minor differences can impact the specificity between ligand and receptor pairs (Nickel et al., 2005). Owing to the availability of only one activin/type I receptor structure (GDF11/ActRIIB/Alk5), a similar comparison has not been made within the activin class (Goebel et al., 2019b). With the resolution of the GDF11/Alk4 complex structure, we can begin to determine how GDF11 is compatible with two different type I receptors by comparison with the previously resolved GDF11/Alk5 structure (Goebel et al., 2019b). These structures may also provide insights for how other ligands, such as ActA or TGFβ, are limited to interaction with a single type I receptor: either Alk4 or Alk5, respectively. Comparison of the two GDF11 structures reveals a similar core interface utilized by both Alk4 and Alk5. Specifically, the Alk4 and Alk5 shared β4β5 N-terminal extension facilitates interactions with the ligand finger 3/4, in addition to similarly engaging the hydrophobic pocket in GDF11 for the knob-in-hole anchoring moiety (Figure 5A). This consensus in fingertip-receptor interactions is highly specific for activin class ligand/receptor binding and is not observed in BMP or TGFβ receptor complexes (Allendorph et al., 2006; Groppe et al., 2008; Radaev et al., 2010; Townson et al., 2012; Weber et al., 2007).

Outside of these conserved interactions, the largest difference in GDF11 binding between Alk4 and Alk5 is observed at the C-terminal region of the β4β5 loop. The Alk5 loop extension is positioned to form hydrogen bonds with both ligand monomers, tethering the loop (Figure 5A). However, as mentioned

earlier, Alk4 lacks this extension and subsequently, is shifted away from the ligand finger 1/2. An additional difference of note is observed in the GDF11 prehelix loop during engagement of Alk4 and Alk5 (Figure S5). While the overall conformation of the prehelix is similar, Tyr347 is flipped away from the β3β4 loop and toward the β4β5 loop in Alk5, facilitated by Lys91 of the β4β5 extension. These differences in the utilization of β4β5 result in an increase in interface area during interaction with Alk5, when compared with Alk4 (736.7Å^2 vs. 940Å^2). These comparisons reveal that the β4β5 loop in both receptors forms the major anchoring interface, but whether these different elements of binding are important for specificity of other ligands is unknown.

To investigate this further, we generated a series of constructs that exchanged either the β3β4 loop or the N-terminal/C-terminal regions of the β4β5 of Alk4 with that of Alk5 and vice versa. Eight residues within the β3β4 region and two sets of eight residues flanking the conserved disulfide bond of the β4β5 loop were selected for the region swaps (Figure 5B). Additionally, the N-terminal and C-terminal swaps were combined in order to generate swaps of the entire β4β5. The effects on ligand specificity and signaling were determined through transfection of the receptors in a luciferase assay. Here, cells were treated with the small molecule inhibitor, SB-431542, to prevent activation of the endogenous activin type I receptors, while the receptor constructs were transfected containing a single intracellular domain mutation, imparting resistance to the small molecule (Ser278Thr and Ser282Thr in Alk4 and Alk5, respectively). Western blots were performed, ensuring relatively equal receptor expression (Figure S6). Following transfection, purified, recombinant ActA, GDF11 or TGFβ1 were assessed for their ability to induce signaling through each receptor. As expected, ActA and GDF11 readily produced signal through Alk4, with TGFβ1 being unable to signal. Replacement of the Alk4 β3β4 loop which engages the prehelix region with that of Alk5 ($Alk4_{\beta3\beta4}$) reduced both ActA and GDF11 signaling by roughly 40%. Expectedly, replacement of the N-terminal region of the Alk4 β4β5 with that of Alk5 ($Alk4_{\beta4\beta5\text{-}N}$), resulted in a reduction of signal for ActA, while GDF11 signaling was maintained. When the C-terminal region was replaced ($Alk4_{\beta4\beta5\text{-}C}$), signaling was maintained for ActA, while GDF11 signaling was slightly increased. Upon complete exchange of the Alk4 β4β5 loop ($Alk4_{\beta4\beta5\text{-}NC}$), ActA signaling was weakened, while GDF11 signaling was maintained. Interestingly, TGFβ1 was able to significantly activate Smad2/3 signaling with the introduction of an Alk5-like β4β5 loop. For Alk5, signaling was also as expected with GDF11 and TGFβ1 robustly signaling and ActA unable to signal. In line with previous trends, Alk4 replacement of the Alk5 β3β4 loop ($Alk5_{\beta3\beta4}$) did not affect signaling in any significant manner. Additionally, replacement of the Alk5 N-terminal β4β5 loop ($Alk5_{\beta4\beta5\text{-}N}$) drastically reduced signaling for each ligand when compared with the $Alk4_{\beta4\beta5\text{-}N}$ construct, which only reduced signaling for ActA. Furthermore, the C-terminal swap in Alk5 ($Alk5_{\beta4\beta5\text{-}C}$) also reduced GDF11 signaling, although to a lesser extent than the N-terminal swap. Lastly, replacement of the entire Alk5 β4β5 loop ($Alk5_{\beta4\beta5\text{-}NC}$) ablated both GDF11 and TGFβ1 signaling. In the end, ActA was unable to signal through any of the Alk5 constructs, despite the introduction of Alk4 regions. However, through the introduction of the Alk5 β4β5 loop into Alk4, TGFβ1 specificity was conferred without entirely losing canonical ActA signaling. Together, these data highlight that the β4β5 of both Alk4 and Alk5 are functionally distinct and not wholly interchangeable. Albeit, coupled with the structural differences observed in the Alk4 and Alk5 complexes, these data highlight that the C-terminal portion of the β4β5 loop likely plays a more important role in ligand interactions and signaling than in Alk4.

DISCUSSION

Several strategies for the inhibition of the TGFβ family of ligands to boost muscle mass have emerged, particularly against members of the activin class. However, candidates targeting a single activin ligand, such as antibodies targeting GDF8 (myostatin), have met with limited success (Latres et al., 2015; Mariot et al., 2017; Singh et al., 2016). This is in part due to functional redundancy with several activin ligands, highlighting the need for broader spectrum inhibitors (Chen et al., 2017; Latres et al., 2017). For example, antibodies directed toward neutralization of the type II receptors have resulted in a greater enhancement to muscle mass (Amato et al., 2014; Lach-trifilieff et al., 2014; Morvan et al., 2017). Recently, an alternative option has been developed that uses a decoy receptor platform, which includes both the type I and type II receptors (ActRIIB-Alk4-Fc) (Li et al., 2021). In animal models, ActRIIB-Alk4-Fc has recently been shown to have a positive impact on muscle mass by specifically inhibiting the activin ligands, Activin A and GDF8, while having a minimal impact on BMP9 signaling. This change in specificity is important as unwanted inhibition of BMP9 was observed with ACE-031 ($(ActRIIB)_2$-Fc) in clinical trials with Duchenne muscular dystrophy patients (Li et al., 2021). In the new decoy receptor format, a type I and a type II receptor mimic the innate signaling complexes of the activin class ligands. Here, we present the structure of this

novel ActRIIB-Alk4 molecule in complex with two different activin ligands, ActA and GDF11. These structures not only represent a snapshot of the therapeutic complex but also powerful tools for understanding how activin ligands and Alk4 interact at the atomic level for the first time.

Given the low affinity between the activins and the type I receptors, we hypothesized that the tethering of Alk4 to the high-affinity type II receptor would favor the formation of a stable complex and would be amenable to crystallization. Comparing the ActRIIB-Alk4-Fc construct with an $(ActRIIB)_2$-Fc and ActRIIB-Fc revealed that in both SPR and cell-based inhibition assays, ActRIIB-Alk4-Fc behaved more similarly to $(ActRIIB)_2$-Fc than ActRIIB-Fc. These observations indicated that the tether was sufficient to facilitate Alk4-ECD participation in ligand binding and set the stage for the resolution of the Alk4 complexes. Given the distance is approximately 40–50 Å from the C-terminal ends of each receptor tail, which are linked by 44 residues missing in the structure, it would seem the linker could be reduced in size and still maintain the ability for both receptors to bind effectively.

Over the past two decades, resolution of ternary complexes involving activin class ligands have lagged behind the resolution of BMP and TGFβ ligand complexes, owing to the low affinity of the type I receptor. Only recently, we reported the structure of the ternary complex of the type I receptor, Alk5, in complex with GDF11 and ActRIIB (Goebel et al., 2019b). This study highlighted that the receptors bind activin ligands independently, similar to what is observed with BMP ligands and in contrast to the cooperative inter-receptor interactions seen with TGFβ ligands (Goebel et al., 2019a). Unlike the BMP receptor complexes, however, significant contacts were observed with the fingertips of the ligand and the β4β5 loop of Alk5 (Goebel et al., 2019b). The current study provides further support that similar interactions also occur with Alk4, indicating that a common theme has evolved to support the binding of low-affinity type I receptors for the activin class. Specifically, the β4β5 loop of both Alk4 and Alk5 form key interactions in the convex cleft centered around two family-conserved tryptophans of the ligand, while additional contacts are formed by both the ligand fingertips and the wrist region (prehelix loop and central helix) with each receptor. For Alk4, this is consistent with previous mutagenesis work that implicated the β4β5 loop as the major ligand-binding site (Harrison et al., 2003). Notably, a major difference between Alk4 and Alk5 is an extension of the β4β5 loop in Alk5 that forms unique ligand interactions with fingers 1 and 2 of GDF11 and is not observed in the structures of Alk4. Thus, while an overall binding mode is similar between Alk4 and Alk5, the receptors exhibit differences at the ligand interface which most likely contribute for differences in ligand specificity.

Previous work to understand ligand/receptor specificity has been largely focused on elements of the ligand. This has led to the identification of the prehelix loop as being a major ligand component important for specificity. In fact, ligands across the family exhibit significant sequence variation in the prehelix loop (Hinck et al., 2016). For example, ActA and ActB have an extended prehelix loop as compared to GDF8 and GDF11. Previous studies have shown that replacing the ActA prehelix with that of GDF8 (~90% similar to GDF11) permitted signaling through Alk5 (Cash et al., 2009). It is worth noting, however, that polyalanine screening of the ActA-GDF8 prehelix loop chimera did not disrupt Alk5 signaling, indicating that the gain of Alk5 signaling was not the result of specific contacts of the prehelix loop of GDF8 and Alk5. This result indicated that the composition and conformation of the prehelix loop play a role in dictating ligand specificity (Cash et al., 2009). The current structures help support these observations, where Alk4 appears to accommodate significantly different prehelix loops of both ActA and GDF11 (Figure 3D). Interestingly, the prehelix loop of ActA adopts a different conformation than in previously determined structures (i.e. bound to the antagonists follistatin or FSTL3) (Stamler et al., 2008; Thompson et al., 2005). Previous structures have shown that this region is highly flexible in the absence of a binding partner (Greenwald et al., 2004; Thompson et al., 2003). Thus, it appears that activin not only goes from a flexible to a restrained state upon binding receptors or antagonists but also that the prehelix can adopt different conformations depending on the binding partner, further supporting the conformational selection model previously proposed for activin class signaling. Because the Fab used for crystallization binds to ActRIIB opposite of ligand binding, we do not anticipate it will influence the ActA of GDF11 conformation. Additionally, the ActA prehelix forms specific interactions with residues of Alk4 that are not conserved in Alk5, such as the formation of additional hydrogen bonds and a saltbridge, suggesting that the ActA prehelix has evolved to select for Alk4 binding over Alk5 binding (Figures 3D and 4B). In contrast, the shorter prehelix of GDF11 adopts a similar conformation and contacts relatively conserved residues during interaction with Alk4 and Alk5 with the only key difference being the altered positioning of Tyr347 (Figure S5).

While the prehelix loop appears to be a major specificity determinant across the broader TGFβ family, recent work has also implicated the ligand fingertip as a region for receptor specificity in the activin class ligands (Aykul et al., 2020; Goebel et al., 2019b). Again, replacement of ActA residues in this region with those of GDF8 or GDF11 conferred Alk5 signaling. The ternary complexes of Alk4 and Alk5 support these observations, as differences are observed in how each receptor interacts with the ligand fingertips. Specifically, a single hydrogen bond is formed between the mainchain of Gly79 in Alk4 and an aspartate in both ActA and GDF11 (Figure 3C), while in Alk5, the glycine is replaced by an aspartate, which forms a more extensive hydrogen bond network specific to the residues of the GDF11 fingertip. Thus, the Alk4 complex structures further support that specific differences at the fingertip-β4β5 interface have important roles in defining which low-affinity type I receptor is engaged for signaling.

While previous studies have focused on understanding what components of the ligand are important for receptor specificity, limited studies have taken the opposite approach and probed which elements of the receptor are important for allowing individual ligands to signal. In this study, we generated a series of Alk4 and Alk5 chimeras and tested the effects on specific ligand signaling. In part, these experiments were designed to determine if there are elements of Alk5 that limit ActA signaling or if there are elements of Alk4 that are important for ActA signaling. As the ActA/Alk4 structure reveals that the prehelix loop and the β3β4 loop uniquely interact, we hypothesized that this region may contribute to specificity; however, swapping the β3β4 between Alk4 and Alk5 did not alter ActA signaling. Moreover, because the majority of the binding interface is derived from interactions with the β4β5 loop, we also performed swaps of this region. Exchange of the Alk4 and Alk5 N-terminal portions of the β4β5 loop resulted in the loss of ActA signaling in the case of the $Alk4_{\beta4\beta5\text{-}N,}$ while largely ablating signaling through $Alk5_{\beta4\beta5\text{-}N}$. This supports that the fingertip-β4β5 interface is a region of specific interaction. However, comparison of the Alk4 and Alk5 sequences in this segment reveals there are only a few non-conserved residues. Inspection of the Alk5 structure reveals an intramolecular contact that tethers the β4β5 N-terminal extension, positioning the loop for interaction with the ligand fingertip (Figure S7). Loss of this interaction might result in a more flexible β4β5 that is unable to interact with the ligands, resulting in a loss of signaling capacity. On the other hand, exchange of the C-terminal β4β5 of Alk5 into Alk4, not only strengthened GDF11 signaling but also generated an Alk4 receptor able to signal with TGFβ. This corroborates with the opposite experiments, in which the ability of Alk5 to bind GDF11 and TGFβ is decreased when the C-terminal β4β5 of Alk4 is introduced. Thus, the β4β5 of Alk5 is critical for ligand binding and is sufficient to generate specificity for TGFβ. This observation is likely due to the introduction of a favorable interface in Alk4 for inter-receptor interactions with the type II receptor, TβRII, indicative of the cooperative receptor assembly of the TGFβ class (Groppe et al., 2008). Overall, exchange of singular receptor regions was unable to alter specificity significantly, especially in the expected case of ActA and the β3β4 swaps. It is possible, however, that these key receptor regions have evolved to act in concert to dictate activin specificity and together, are compatible for ligand binding.

The resolution of both ActA/ActRIIB-Alk4 and GDF11/ActRIIB-Alk4 highlights that incorporation of both a type I and type II receptor fused to an Fc can effectively interact with a ligand to mimic the cognate signaling complex. Given that this new platform has beneficial effects in mouse models of muscle pathologies, this study provides molecular information that can be used to help optimize binding interactions to alter ligand affinity or specificity. For instance, introducing the Alk5 C-terminal β4β5 region into Alk4 may enhance GDF11 binding, and in turn, inhibition. Additionally, these structures offer the opportunity to directly compare how Alk4 binds two activin ligands, expanding our understanding of how activin/type I receptor specificity is derived. Given the success of this platform in providing an avenue for circumventing the low-affinity interactions between Alk4 and the ligands, a similar strategy might be used to explore the interactions between the activins and two other type I receptors, Alk2 and Alk7, which have yet to be structurally characterized.

Limitations of the study

This study concerns itself primarily with structural and functional studies within the limited realms of biochemistry and cell-based *in vitro* systems. Accordingly, there is no attention given to the effect of ActRIIB-Alk4-Fc in a more complicated biological model system, although these questions are addressed in other publications. However, there are also certain crystallographic limitations within the scope of the study that must be considered. Both of the structures presented here are bound to an antibody Fab, which

may induce some non-native conformational changes in the complex structure that would be difficult to account for. In addition, one question that we were hoping to address was whether the ActRIIB-Alk4-Fc preferentially binds to the ligands in a cis or *trans* orientation, or if there is a mixture of conformations. However, the linker regions are not visible within the election density for either structure. Additionally, the linker regions attaching the receptor ECDs to the Fc are of sufficient length as to conceivably conform to either a cis or a *trans* binding orientation.

STAR★METHODS

Detailed methods are provided in the online version of this paper and include the following:

- KEY RESOURCES TABLE
- RESOURCE AVAILABILITY
  - Lead contact
  - Materials availability
  - Data and code availability
- EXPERIMENTAL MODEL AND SUBJECT DETAILS
  - Cell lines
- METHOD DETAILS
  - Recombinant protein expression and purification
  - Complex formation
  - Crystallization and structure determination
  - Surface plasmon resonance
  - Luciferase reporter assays
- QUANTIFICATION AND STATISTICAL ANALYSIS

SUPPLEMENTAL INFORMATION

Supplemental information can be found online at https://doi.org/10.1016/j.isci.2021.103590.

ACKNOWLEDGMENTS

The authors would like to thank Adimab for the Anti-ActRIIB antibody as well as members of the Acceleron Protein Sciences group for generating reagents for this study. Additionally, we thank Nadia Rose at SARomics for complex preparation of the ActA structure. This study was funded byNIH R35 GM134923.

AUTHOR CONTRIBUTIONS

E.J.G., C.K., L.K., A.V.G., R.C, R.K., and T.B.T designed research; E.J.G, C.K., L.K., M.C., M.C., M.C.M., R.G., M.H, D.S., and D.T.L performed research; E.J.G., G.R.G, M.C., R.C., R.K., and T.B.T. analyzed data; and E.J.G., G.R.G., and T.B.T. wrote the paper.

DECLARATION OF INTERESTS

T.B.T. is a consultant for Acceleron Pharma, a wholly owned subsidiary of Merck &Co., Inc.. R.C., R.G., L.K., M.C., M.C.M., D.S., and R.K. are current employees of Acceleron Pharma, a wholly owned subsidiary of Merck &Co., Inc.. M.H. and D.T.L. are current employees of SARomics Biostructures. The other authors declare no competing interests.

Received: July 23, 2021
Revised: November 18, 2021
Accepted: December 6, 2021
Published: January 21, 2022

REFERENCES

Afonine, P.V., Grosse-Kunstleve, R.W., Echols, N., Headd, J.J., Moriarty, N.W., Mustyakimov, M., Terwilliger, T.C., Urzhumtsev, A., Zwart, P.H., and Adams, P.D. (2012). Towards automated crystallographic structure refinement with phenix.refine. Acta Crystallogr.Sect. D Biol. Crystallogr. *68*, 352–367.

Allendorph, G.P., Vale, W.W., and Choe, S. (2006). Structure of the ternary signaling complex of a TGF-beta superfamily member. Proc. Natl. Acad. Sci.U S A *103*, 7643–7648.

Amato, A.A., Sivakumar, K., Goyal, N., David, W.S., Salajegheh, M., Praestgaard, J., Lach-

Trifilieff, E., Trendelenburg, A.-U., Laurent, D., Glass, D.J., et al. (2014). Treatment of sporadic inclusion body myositis with bimagrumab. Neurology *83*, 2239–2246.

Attisano, L., Cárcamo, J., Ventura, F., Weis, F.M.B., Massagué, J., and Wrana, J. (1993).

Identification of human activin and TGF beta type I receptors that form heteromeric kinase complexes with type II receptors. Cell *75*, 671–680.

Aykul, S., Corpina, R.A., Goebel, E.J., Cunanan, C.J., Dimitriou, A., Kim, H.J., Zhang, Q., Rafique, A., Leidich, R., Wang, X., et al. (2020). Activin a forms a non-signaling complex with ACVR1 and type II Activin/BMP receptors via its finger 2 tip loop. Elife *9*, 1–19.

Badarau, A., Rouha, H., Malafa, S., Battles, M.B., Walker, L., Nielson, N., Dolezilkova, I., Teubenbacher, A., Banerjee, S., Maierhofer, B., et al. (2016). Context matters: the importance of dimerization-induced conformation of the LukGH leukocidin of Staphylococcus aureus for the generation of neutralizing antibodies. MAbs *8*, 1347–1360.

Cadena, S.M., Tomkinson, K.N., Monnell, T.E., Spaits, M.S., Kumar, R., Underwood, K.W., Pearsall, R.S., and Lachey, J.L. (2010). Administration of a soluble activin type IIB receptor promotes skeletal muscle growth independent of fiber type. J. Appl. Physiol. *109*, 635–642.

Cash, J.N., Rejon, C.A., McPherron, A.C., Bernard, D.J., and Thompson, T.B. (2009). The structure of myostatin:follistatin 288: insights into receptor utilization and heparin binding. EMBO J. *28*, 2662–2676.

Chen, J.L., Walton, K.L., Hagg, A., Colgan, T.D., Johnson, K., Qian, H., Gregorevic, P., and Harrison, C.A. (2017). Specific targeting of TGF-β family ligands demonstrates distinct roles in the regulation of muscle mass in health and disease. Proc. Natl. Acad. Sci. U S A *114*, E5266–E5275.

Emsley, P., Lohkamp, B., Scott, W.G., and Cowtan, K. (2010). Features and development of Coot. Acta Crystallogr.Sect. D Biol. Crystallogr. *66*, 486–501.

Evans, P.R., and Murshudov, G.N. (2013). How good are my data and what is the resolution? Acta Crystallogr.Sect. D Biol. Crystallogr. *69*, 1204–1214.

Goebel, E.J., Hart, K.N., McCoy, J.C., and Thompson, T.B. (2019a). Structural biology of the TGFβ family. Exp. Biol. Med. *244*, 1530–1546.

Goebel, E.J., Corpina, R.A., Hinck, C.S., Czepnik, M., Castonguay, R., Grenha, R., Boisvert, A., Miklossy, G., Fullerton, P.T., Matzuk, M.M., et al. (2019b). Structural characterization of an activin class ternary receptor complex reveals a third paradigm for receptor specificity. Proc. Natl. Acad. Sci. *116*, 15505–15513.

Greenwald, J., Vega, M.E., Allendorph, G.P., Fischer, W.H., Vale, W., and Choe, S. (2004). A flexible activin explains the membrane-dependent cooperative assembly of TGF-β family receptors. Mol. Cell *15*, 485–489.

Groppe, J., Hinck, C.S., Samavarchi-Tehrani, P., Zubieta, C., Schuermann, J.P., Taylor, A.B., Schwarz, P.M., Wrana, J.L., and Hinck, A.P. (2008). Cooperative assembly of TGF-β superfamily signaling complexes is mediated by two disparate mechanisms and distinct modes of receptor binding. Mol. Cell *29*, 157–168.

Harrington, A.E., Morris-Triggs, S.A., Ruotolo, B.T., Robinson, C.V., Ohnuma, S.I., and Hyvönen, M. (2006). Structural basis for the inhibition of activin signalling by follistatin. EMBO J. *25*, 1035–1045.

Harrison, C.A., Gray, P.C., Koerber, S.C., Fischer, W., and Vale, W. (2003). Identification of a functional binding site for activin on the type I receptor ALK4. J. Biol. Chem. *278*, 21129–21135.

Hinck, A.P. (2012). Structural studies of the TGF-betas and their receptors - insights into evolution of the TGF-beta superfamily. FEBS Lett. *586*, 1860–1870.

Hinck, A.P., Mueller, T.D., and Springer, T.A. (2016). Structural biology and evolution of the TGF-β family. Cold Spring Harb. Perspect. Biol. *8*, 1–51.

Kabsch, W. (2010). XDS. Acta Crystallogr. D. Biol. Crystallogr. *66*, 125–132.

Klages, J., Kotzsch, A., Coles, M., Sebald, W., Nickel, J., Müller, T., and Kessler, H. (2008). The solution structure of BMPR-IA reveals a local disorder-to-order transition upon BMP-2 binding. Biochemistry *47*, 11930–11939.

Kotzsch, A., Nickel, J., Seher, A., Sebald, W., and Müller, T.D. (2009). Crystal structure analysis reveals a spring-loaded latch as molecular mechanism for GDF-5-type I receptor specificity. EMBO J. *28*, 937–947.

Kumar, R., Grinberg, A.V., Li, H., Kuo, T.H., Sako, D., Krishnan, L., Liharska, K., Li, J., Grenha, R., Maguire, M.C., et al. (2021). Functionally diverse heteromeric traps for ligands of the transforming growth factor-β superfamily. Sci. Rep. *11*, 1–16.

Lach-trifilieff, E., Minetti, G.C., Sheppard, K., Ibebunjo, C., Feige, J.N., and Hartmann, S. (2014). An antibody blocking activin type II receptors induces strong skeletal muscle hypertrophy and protects from atrophy. Mol. Cell Biol. *34*, 606–618.

Latres, E., Pangilinan, J., Miloscio, L., Bauerlein, R., Na, E., Potocky, T.B., Huang, Y., Eckersdorff, M., Rafique, A., Mastaitis, J., et al. (2015). Myostatin blockade with a fully human monoclonal antibody induces muscle hypertrophy and reverses muscle atrophy in young and aged mice. Skelet. Muscle *5*, 34–47.

Latres, E., Mastaitis, J., Fury, W., Miloscio, L., Trejos, J., Pangilinan, J., Okamoto, H., Cavino, K., Na, E., Papatheodorou, A., et al. (2017). Activin A more prominently regulates muscle mass in primates than does GDF8. Nat. Commun. *8*, 15153–15166.

Li, J., Fredericks, M., Cannell, M., Wang, K., Sako, D., Maguire, M.C., Grenha, R., Liharska, K., Krishnan, L., Bloom, T., et al. (2021). ActRIIB:ALK4-Fc alleviates muscle dysfunction and comorbidities in murine models of neuromuscular disorders. J. Clin. Invest. *131*, 138634–138650.

Mariot, V., Joubert, R., Hourdé, C., Féasson, L., Hanna, M., Muntoni, F., Maisonobe, T., Servais, L., Bogni, C., Le Panse, R., et al. (2017). Downregulation of myostatin pathway in neuromuscular diseases may explain challenges of anti-myostatin therapeutic approaches. Nat. Commun. *8*, 6–13.

McCoy, A.J., Grosse-Kunstleve, R.W., Adams, P.D., Winn, M.D., Storoni, L.C., and Read, R.J. (2007). Phaser crystallographic software. J. Appl. Crystallogr. *40*, 658–674.

Morvan, F., Rondeau, J.-M., Zou, C., Minetti, G., Scheufler, C., Scharenberg, M., Jacobi, C., Brebbia, P., Ritter, V., Toussaint, G., et al. (2017). Blockade of activin type II receptors with a dual anti-ActRIIA/IIB antibody is critical to promote maximal skeletal muscle hypertrophy. Proc. Natl. Acad. Sci. U S A *114*, 12448–12453.

Murshudov, G.N., Skubák, P., Lebedev, A.A., Pannu, N.S., Steiner, R.A., Nicholls, R.A., Winn, M.D., Long, F., and Vagin, A.A. (2011). REFMAC5 for the refinement of macromolecular crystal structures. Acta Crystallogr.Sect. D Biol. Crystallogr. *67*, 355–367.

Nickel, J., Kotzsch, A., Sebald, W., and Mueller, T.D. (2005). A single residue of GDF-5 defines binding specificity to BMP receptor IB. J. Mol. Biol. *349*, 933–947.

Oganesyan, V., Peng, L., Bee, J.S., Li, J., Perry, S.R., Comer, F., Xu, L., Cook, K., Senthil, K., Clarke, L., et al. (2018). Structural insights into the mechanism of action of a biparatopic anti-HER2 antibody. J. Biol. Chem. *293*, 8439–8448.

Puolakkainen, T., Ma, H., Kainulainen, H., Pasternack, A., Rantalainen, T., Ritvos, O., Heikinheimo, K., Hulmi, J.J., and Kiviranta, R. (2017). Treatment with soluble activin type IIB-receptor improves bone mass and strength in a mouse model of Duchenne muscular dystrophy. BMC Musculoskelet. Disord. *18*, 20–31.

Radaev, S., Zou, Z., Huang, T., Lafer, E.M., Hinck, A.P., and Sun, P.D. (2010). Ternary complex of transforming growth factor-β1 reveals isoform-specific ligand recognition and receptor recruitment in the superfamily. J. Biol. Chem. *285*, 14806–14814.

Sako, D., Grinberg, A.V., Liu, J., Davies, M.V., Castonguay, R., Maniatis, S., Andreucci, A.J., Pobre, E.G., Tomkinson, K.N., Monnell, T.E., et al. (2010). Characterization of the ligand binding functionality of the extracellular domain of activin receptor type IIB. J. Biol. Chem. *285*, 21037–21048.

Salmon, R.M., Guo, J., Wood, J.H., Tong, Z., Beech, J.S., Lawera, A., Yu, M., Grainger, D.J., Reckless, J., Morrell, N.W., et al. (2020). Molecular basis of ALK1-mediated signalling by BMP9/BMP10 and their prodomain-bound forms. Nat. Commun. *11*, 1–16.

Singh, P., Rong, H., Gordi, T., Bosley, J., and Bhattacharya, I. (2016). Translational pharmacokinetic/pharmacodynamic analysis of MYO-029 antibody for muscular dystrophy. Clin. Transl. Sci. *9*, 302–310.

Stamler, R., Keutmann, H.T., Sidis, Y., Kattamuri, C., Schneyer, A., and Thompson, T.B. (2008). The structure of FSTL3·activin A complex: differential binding of N-terminal domains influences follistatin-type antagonist specificity. J. Biol. Chem. *283*, 32831–32838.

Thompson, T.B., Woodruff, T.K., and Jardetzky, T.S. (2003). Structures of an ActRIIB:activin A complex reveal a novel binding mode for TGF-beta ligand:receptor interactions. EMBO J. *22*, 1555–1566.

Thompson, T.B., Lerch, T.F., Cook, R.W., Woodruff, T.K., and Jardetzky, T.S. (2005). The structure of the follistatin:activin complex reveals antagonism of both type I and type II receptor binding. Dev. Cell *9*, 535–543.

Townson, S.A., Martinez-Hackert, E., Greppi, C., Lowden, P., Sako, D., Liu, J., Ucran, J.A., Liharska, K., Underwood, K.W., Seehra, J., et al. (2012). Specificity and structure of a high affinity activin receptor-like kinase 1 (ALK1) signaling complex. J. Biol. Chem. *287*, 27313–27325.

Walker, R.G., Czepnik, M., Goebel, E.J., McCoy, J.C., Vujic, A., Cho, M., Oh, J., Aykul, S., Walton, K.L., Schang, G., et al. (2017). Structural basis for potency differences between GDF8 and GDF11. BMC Biol. *15*, 19–41.

Waterhouse, A., Bertoni, M., Bienert, S., Studer, G., Tauriello, G., Gumienny, R., Heer, F.T., De Beer, T.A.P., Rempfer, C., Bordoli, L., et al. (2018). SWISS-MODEL: homology modelling of protein structures and complexes. Nucleic Acids Res. *46*, W296–W303.

Weber, D., Kotzsch, A., Nickel, J., Harth, S., Seher, A., Mueller, U., Sebald, W., and Mueller, T.D. (2007). A silent H-bond can be mutationally activated for high-affinity interaction of BMP-2 and activin type IIB receptor. BMC Struct. Biol. *7*, 6–26.

Weiss, A., and Attisano, L. (2013). The TGFbeta superfamily signaling pathway. Wiley Interdiscip. Rev. Dev. Biol. *2*, 47–63.

Wrana, J.L., Attisano, L., Wieser, R.R., Ventura, F., Massagué, J., and Massague, J. (1994). Mechanism of activation of the TGF-β receptor. Nature *370*, 341–347.

Zou, Z., and Sun, P.D. (2004). Overexpression of human transforming growth factor-β1 using a recombinant CHO cell expression system. Protein Expr. Purif. *37*, 265–272.

Zuniga, J.E., Groppe, J.C., Cui, Y., Hinck, C.S., Contreras-Shannon, V., Pakhomova, O.N., Yang, J., Tang, Y., Mendoza, V., López-Casillas, F., et al. (2005). Assembly of TβRI:TβRII:TGFβ ternary complex in vitro with receptor extracellular domains is cooperative and isoform-dependent. J. Mol. Biol. *354*, 1052–1068.

Zuniga, J.E., Ilangovan, U., Mahlawat, P., Hinck, C.S., Huang, T., Groppe, J.C., McEwen, D.G., and Hinck, A.P. (2011). The TβR-I pre-helix extension is structurally ordered in the unbound form and its flanking prolines are essential for binding. J. Mol. Biol. *412*, 601–618.

STAR★METHODS

KEY RESOURCES TABLE

REAGENT or RESOURCE	SOURCE	IDENTIFIER
Antibodies		
Goat monoclonal anti-human IgG (Fc specific)	Sigma	Cat#:I2136; RRID:AB_260147
Rabbit monoclonal anti-HA, HRP conjugated	R&D	Cat#:HAM0601
Rabbit monoclonal anti-Flag, HRP conjugated	R&D	Cat#:HAM85291
Mouse monoclonal anti-Actin, HRP conjugated	Proteintech	Cat#:HRP-60008
Bacterial and virus strains		
BaculoGold baculovirus	BDPharmingen	N/A
Chemicals, peptides, and recombinant proteins		
ActRIIB ECD	Produced by authors	N/A
ActRIIB-Fc	Produced by authors	N/A
$(ActRIIB)_2$-Fc	Produced by authors	N/A
ActRIIB-Alk4-Fc	Produced by authors	N/A
GDF11 mature	Produced by authors	N/A
Activin A mature	Produced by authors	N/A
TGFβ-1 mature	Produced by authors	N/A
Critical commercial assays		
Dual-Luciferase Reporter Assay	Promega	Cat# E1910
Luciferase Reporter Assay	Promega	Cat#: E1500
Deposited data		
ActA/ActRIIB/Alk4/Fab structure	This paper	PDB: 7OLY
GDF11/ActRIIB/Alk4/Fab structure	This paper	PDB: 7MRZ
Experimental models: Cell lines		
SF9	Protein Sciences Corp.	RRID:CVCL_0549
ExpresSF+	Protein Sciences Corp.	N/A
CHO	ATCC	RRID:CVCL_K173
ExpiCHO-S	Gibco	RRID:CVCL_5J31
CHO DUKX	ATCC	RRID:CVCL_1977
HEK-293-$(CAGA)_{12}$	Who knows, ask Chandra	RRID:CVCL_ZD63
A204	ATCC	RRID:CVCL_1058
Software and algorithms		
XDS	Kabsch (2010)	https://xds.mr.mpg.de/
Phaser	McCoy et al. (2007)	https://phenix-online.org/
Aimless	Evans and Murshudov (2013)	https://www.ccp4.ac.uk/
Phenix Refine	Afonine et al. (2012)	https://phenix-online.org/
Buster	Global Phasing Institute	https://www.globalphasing.com/buster/
Refmac5	Murshudov et al. (2011)	https://www.ccp4.ac.uk/
Coot	Emsley et al.,(2010)	https://www2.mrc-lmb.cam.ac.uk/personal/pemsley/coot/
Swiss-Model	Waterhouse et al. (2018)	https://swissmodel.expasy.org/

RESOURCE AVAILABILITY

Lead contact

Further information and requests for resources and reagents should be directed to and will be fulfilled by the lead contact, Thomas B. Thompson (Tom.Thompson@uc.edu).

Materials availability

This study did not generate new unique reagents.

Data and code availability

1. Data

Structural data have been deposited at the Protein Data Bank and are publically available as of the date of publication. Accession numbers are listed in the key resources table.

All other data reported in this paper will be shared by the lead contact upon request.
2. Code

This paper does not report original code.
3. Additional information

Any additional information required to reanalyze the data reported in this paper is available from the lead contact upon request.

EXPERIMENTAL MODEL AND SUBJECT DETAILS

Cell lines

The following cells lines were used to produce recombinant protein:SF9 cells (RRID:CVCL_0549, female Spodoptera frugiperda), cultured in SFf-900 II Serum-free medium (Gibco) at 27°C.

ExpresSF+ cells (female Spodoptera frugiperda), cultured in Sf-900 II Serum-free medium (Gibco) at 27°C.

CHO cells (RRID:CVCL_K173, female Cricetulus griseus ovary), cultured in CHO-S-SFM II (Gibco) at 37°C in 5% CO_2.

ExpiCHO-S cells (RRID:CVCL_5J31, female Cricetulus griseus ovary), cultured in ExpiCHO Expression Medium (Gibco) at 37°C in 5% CO_2.

CHO DUKX cells (RRID:CVCL_1977, female Cricetulus griseus ovary), cultured in Iscove's modified Dulbecco's medium with 4 mM L-glutamine and 1.5 g/L sodium bicarbonate (Corning), supplemented with 0.1 mM hypoxanthine, 0.016 mM thymidine, 0.002mM Methotrexate (Amethopterin) and 10% FBS at 37°C in 5% CO_2.

The following cell lines were used to perform *in vitro* Luciferase Reporter Assays:

HEK-293-$(CAGA)_{12}$ luciferase reporter cells (RRID:CVCL_ZD63, female Homo sapiens kidney), cultured in Dubecco's Modified Eagle Medium with high glucose and L-glutamate (Corning), supplemented with 10% fetal bovine serum (FBS), 1x Penicillin/Streptavidin and 100µg/mL G418 at 37°C in 5% CO_2.

A204 cells (RRID:CVCL_1058, female Homo sapiens muscle), cultured in McCoy's Medium (Gibco) supplemented with 10% FBS at 37°C in 5% CO_2.

METHOD DETAILS

Recombinant protein expression and purification

The extracellular domain of rat ActRIIB (residues 1-120) was prepared as previously described (Goebel et al., 2019b; Thompson et al., 2003). Briefly, ActRIIB was cloned into the pVL1392 baculovirus vector with a C-terminal thrombin cleavage site followed by a His_6 tag. Initial recombinant baculovirus was

produced through the Baculogold system (Pharmingen) and amplified in SF9 insect cells (Protein Sciences Corp). Protein production was carried out in ExpresSF+ insect cells (Protein Sciences Corp), followed by purification of the conditioned medium (CM) over a Ni Sepharose affinity resin (GE healthcare) with buffers containing 50mM Na_2HPO_4 pH 7.5, 500mM NaCl, and 20/500mM Imidazole for load + wash/elution. Following an overnight thrombin digestion, ActRIIB-ECD was then loaded through a HiLoad Superdex S75 16/60 size exclusion column (SEC, GE healthcare) in 20mM HEPES pH 7.4 and 500mM NaCl (SEC buffer).

$(ActRIIB)_2$-Fc and ActRIIB-Fc were expressed and purified from Chinese hamster ovary (CHO) cells as previously described for $(ActRIIB)_2$-Fc (Cadena et al., 2010; Sako et al., 2010). In brief, serum-free CM produced from stably transfected CHO cells was purified by affinity chromatography using MAB SelectSureProtienA resin (GE Heathcare), and a glycine elution. Semi-purified protein was then further purified by ion exchange chromatography, using a Q-Sepharose column (GE Healthcare) and eluted with an NaCl gradient. ActRIIB-Alk4-Fc was expressed and purified as recently described, with the addition of kifunensine in the CHO expression media to reduce glycosylation heterogeneity (Li et al., 2021). In brief, filtered serum-free CM from stably transfected CHO DUKX cells was purified by affinity chromatography using MAB SelectSureProtienA resin (GE Heathcare). Semi-purified protein was then further purified sequentially by His affinity chromatography (using a Ni Sepharose 6 FastFlow column (GE Healthcare) eluted with an imidazole gradient) and ion exchange chromatography (using a Q-Sepharose column (GE Healthcare) and eluted with an NaCl gradient). The anti-ActRIIB antibody was transiently expressed in ExpiCHO cells (ThermoFisher) using manufacturer's protocol, followed by a purification over Protein A (MAb SelectSuRe, Cytiva) and cation-exchange (SP, Cytiva) chromatography columns.

Mature, recombinant ActA, GDF11 and TGFβ1 were prepared as previously described (Goebel et al., 2019b; Zou and Sun, 2004). Briefly, ActA and GDF11 were cloned into the pAID4T vector, containing a UCOE element (Millipore). Then, expression was performed in Chinese hamster ovary (CHO) DUKX cells and pools were generated based on expression of ActA and GDF11. Conditioned media (CM) of ActA was then mixed with a proprietary affinity resin made with an ActRIIA-related construct (Acceleron). The resin was then lowered to a pH of 3 to dissociate the propeptide-ligand complex. Following this, the pH was raised to 7.5 and the resin was incubated for 2h at room temperature. ActA was eluted with 0.1M glycine pH 3.0, which was concentrated over a phenyl hydrophobic interaction column (GE Healthcare) and eluted with 50% acetonitrile/water with 0.1% trifluoroacetic acid (TFA). Lastly, amicon-concentrated sample was further purified over a preparative reverse phase C4 column (Vydac) through HPLC with a gradient of water/0.1% TFA and acetonitrile/0.1% TFA. Fractions containing pure, recombinant ActA were pooled and lyophilized to be resuspended in 10mM HCl for future experimentation. GDF11 CM was filtered, concentrated and heated to 75°C prior to cooling and initial purification through incubation for 2h with a proprietary affinity resin based on an ActRIIB-related construct. Following a wash with PBS and elution with 0.1M Glycine pH 3.0, GDF11 was purified over a C4 reverse-phase column and lyophilized, as described with ActA. Human TGF-β1 was expressed and purified from CM produced by a stably transfected CHO line as described previously (Zou and Sun, 2004). In brief, filtered CM from these cells was purified over a Ni-NTA agarose column, equilibrated with 50 mM Tris–HCl and 150 mM NaCl at pH 8.0, and then eluted with an imidazole gradient. Protein containing fractions were then pooled, pH adjusted to 3.0, concentrated, and then ultimately purified by Size Exclusion Chromatography using HiLoad 16/60 Superdex 200 column (Amersham Biosciences) with equilibrated with 50 mM glycine pH 4.0 with 50 mM NaCl. Fractions containing pure, recombinant TGF-β1 were pooled and lyophilized to be resuspended in 10mM HCl for future experimentation.

Complex formation

In order to generate the GDF11/ActRIIB-Alk4/anti-ActRIIB complex, purified ActRIIB-Alk4-Fc was digested with IdeS-His for 6 h, cleaving below the hinge sequence and removing the Fc. Following this, GDF11 was supplemented at a 1:2 ligand:receptor molar ratio to favor complex formation, which, following a 20min incubation at room temperature, was purified over an SRT-10 SEC300 column (Sepax) in 20mM HEPES pH 7.5, 500mM NaCl run at 7mL/min. Following concentration, the complex was subjected to a mixture of deglycosylation enzymes: Deglycomx, Endo-H, OglyZor (QA-bio) at 37°C for ~1 week. In parallel, the anti-ActRIIB antibody was digested with papain at 37°C for 7 hours in 100mM NaAcetate pH 5.5, 8mM cysteine, and 1mM EDTA. The Fab fragments were then purified over a SCX-column in 20mM Na_2HPO_4 pH 6 and eluted with a gradient of 0-30% 20mM Na_2HPO_4 pH 6, 500mM NaCl over 60 min. The Fab product

was then dialyzed in 20mM HEPES, 150mM NaCl pH 7.5, added to the deglycosylated GDF11/ActRIIB:Alk4 complex at a 2:1 Ab:complex ratio and finally purified over a SRT-10 SEC300 in 20mM HEPES pH 7.5, 500mM NaCl at a flow rate of 7mL/min.

In order to generate the ActA/ActRIIB-Alk4/anti-ActRIIB complex, the Fc was cleaved using a FabRICATOR kit (Genovis) where the resin was equilibrated in 20mM NaPO4, 150mM NaCl pH 7.4 and the sample, incubated for 30 min at room temperature followed by collection through centrifugation. The digested sample was then cleaned on CaptureSelect resin (Thermo) to remove the Fc-tag and the nondigested protein. To further purify ActRIIB-Alk4, the sample was loaded on Superdex 200 (26/60) (Sigma) pre-equilibrated in SEC buffer (20 mM Tris, 200 mM NaCl, pH 7.5. For complex formation, purified ActRIIB-Alk4 was mixed with ActA at a 1:2.1 ligand:receptor molar ratio and incubated on ice for 1 hour. Complex was purified through SEC on the Superdex 200 (26/60) column. In parallel, the monoclonal anti-ActRIIB was concentrated to 6.6mg/ml and cleaved using immobilized FabALACTICA (Genovis) to produce a Fab fragment. To remove the Fc part and the nondigested mAb, the digested antibody was applied on a CaptureSelect resin pre-equilibrated in PBS. For complex formation, the purified ActA/ActRIIB-Alk4 was mixed with the purified Fab fragments at a 1:1.3 molar ratio and incubated on ice for 1 hour prior to purification though SEC with the Superdex 200 (26/60) column.

Crystallization and structure determination

The purified GDF11 and ActA/ActRIIB-Alk4/Fab complexes were concentrated to 10mg/mL and 17.7mg/mL, respectively, and used to initiate crystallization trials using vapor diffusion. The final GDF11 complex crystal was grown in mother liquor consisting of 0.1M HEPES pH 7, 0.9M $AmSO_4$ and 0.9M KCl at 20°C using the hanging drop method. The final ActA complex crystal was grown in mother liquor of 0.1M Na cacodylate pH 6.5 and 17% (w/v) PEG 4000. Mother liquor supplemented with 25% glycerol (GDF11 complex) or 30% glycerol (ActA) was used as the cryo-protectant for crystal freezing. For GDF11/ActRIIB-Alk4/Fab, X-ray diffraction data were collected at GM-CA beamline 23-ID-B of the Advanced Photon Source at Argonne National Laboratory with an Eiger 16M detector. For ActA/ActRIIB-Alk4/Fab, data were collected at 100K at station BioMAX, MAX IV Laboratory, Sweden (λ = 0.992 Å) equipped with an Eiger 16M detector. For both structures, data Indexing and integration were performed within XDS followed by subsequent scaling and merging through AIMLESS (Evans and Murshudov, 2013; Kabsch, 2010). Placement of the complete complexes was performed through molecular replacement within Phaser by using the search models: GDF11/ActRIIB (PDB: 6MAC), ActA (PDB:2ARV), an Alk4 model built from closest relative, Alk5 (PDB: 6MAC) and an anti-ActRIIB Fab model was built from sequence and close homolog (GDF11, PDB: 6ATT or ActA, PDB: 5K59 with the CDR loops removed) (Badarau et al., 2016; Goebel et al., 2019b; Harrington et al., 2006; McCoy et al., 2007; Oganesyan et al., 2018). Both models were built using SwissModel (Waterhouse et al., 2018). Final refinement was performed with either Phenix.Refine (GDF11) or Buster and Refmac5 (ActA) software with final model building in Coot (Afonine et al., 2012; Emsley et al., 2010; Murshudov et al., 2011). Structure coordinates were deposited and are publicly available in the PDB under codes, 7MRZ (GDF11) and 7OLY (ActA).

Surface plasmon resonance

Anti-human IgG (Fc specific) antibody (Sigma, Cat# I2136) was immobilized via amine-coupling to a density of ~5000 RU on flow cells 1-4 of a CM5 biosensor chip (Cytiva). Each receptor-Fc construct was diluted in HBS-EP(+) buffer (Cytiva), supplemented with 0.5mg/mL BSA (Sigma) + 350mM NaCl, with a target capture level of ~70 RU. A 9-step, 2-fold serial dilution was performed in the aforementioned buffer for each ligand, with an initial concentration of 10nM. Experiments were conducted at 25°C on a Biacore™ T100 (GE Healthcare) instrument with an association and dissociation time of 360 and 900 seconds, respectively. The flow rate for kinetics was maintained at 50µL/min. Kinetic analysis was conducted using the Biacore™ T200 Evaluation Software using a 1:1 fit model.

Luciferase reporter assays

Assays using the HEK-293-$(CAGA)_{12}$ luciferase reporter cells (initially derived from RRID:CVC:0045) were performed similarly as previously reported (Goebel et al., 2019b; Walker et al., 2017). In brief, cells were plated in a 96-well format (3 x 10^4 cells/well) and grown for 24h. For the inhibition experiments involving the differential forms of ActRIIB (Figure 1C), the growth media was removed 24 h post-plating and replaced with serum free media containing 0.1% BSA, a constant ligand (ActA, GDF11) concentration (0.62nM) and a twofold serial dilution of either ActRIIB-ECD, homodimeric $(ActRIIB)_2$-Fc or ActRIIB-Alk4-Fc

(0.155 - 79.36nM) for 18 h. Cells were then lysed and assayed for luminescence using the Luciferase Reporter Assay System (Promega) and a Synergy H1 Hybrid plate reader (BioTek). For the assays featuring Alk4 and Alk5 mutagenesis in Figure 5, a total of 50ng DNA containing either wildtype or mutant receptor (pRK5 rat Alk5 Ser278Thr (ST) or pcDNA3 rat Alk4 Ser282Thr) was transfected using Mirus LT-1 transfection reagent at 24 h post-plating. The corresponding empty vector was added to normalize the total DNA concentration. Media was then removed and replaced with serum free media containing 0.1% BSA, ligand (ActA, GDF11, TGFβ1) at a constant concentration (0.62nM) and 10uM SB-431542. Cells were lysed and luminescence was measured following 18 h of treatment.

Assays for Figure S1 were performed by Acceleron in A204 cells as previously reported (Kumar et al., 2021). In brief, cells were plated in a 96-well format (1 x 10^5 cells/well) and grown overnight. Cells were then transfected with the pGL3 CAGA12 firefly luciferase reporter plasmid and a control pRL-CMV renilla luciferase reporter plasmid using X-tremeGENE 9 (Roche) in serum free medium with 0.1% BSA. 24 h post transfection, cells were treated with a constant ligand (ActA, GDF11) concentration (0.192nM) and a threefold serial dilution of either monomeric ActRIIB-FC (0.07 – 153nm), homodimeric $(ActRIIB)_2$-Fc (0.0009 – 1.9nM) or ActRIIB-Alk4-Fc (0.006 – 13.2nM) for 6 h. Cells were then lysed and assayed for luminescence using the Dual-Luciferase Reporter Assay System (Promega) and a Synergy H1 Hybrid plate reader (BioTek).

QUANTIFICATION AND STATISTICAL ANALYSIS

For SPR, kinetic analysis was conducted using the Biacore™ T200 Evaluation Software using a 1:1 fit model with mass transport limitations. Each experiment was performed in triplicate and the kinetic parameters were averaged and reported in Table S1.

For Luciferase Reporter Assays, data was plotted using GraphPad Prism. Pooled data from N = 3 separate experiments and Standard Deviation is shown. For inhibition assays (Figures 1C and S1), data was fit with a nonlinear regression with variable slope.